Adaptive Manipulation of a Hybrid Mechanism Mobile Robot

Paul M. Moubarak
Robotics and Mechatronics Laboratory
Mechanical and Aerospace Engineering
The George Washington University
Washington, DC, USA
e-mail: paul4@gwmail.gwu.edu

Pinhas Ben-Tzvi
Robotics and Mechatronics Laboratory
Mechanical and Aerospace Engineering
The George Washington Unviersity
Washington, DC, USA
e-mail: bentzvi@gwu.edu

***Abstract*— This paper reports experimental and analytical results of a Hybrid Mechanism Mobile Robot (HMMR) designed for field and military applications. The HMMR presented in this paper constitutes the second generation of a mobile robot that combines locomotion with manipulation in a symmetric invertible platform. The experimental results highlight the ability of the robot to operate in an unstructured environment and overcome obstacles that are much taller than its folded structure. The analytical results on the other hand reflect the ability of the robot to adapt the arm's posture to the magnitude of the external load during manipulation in order to prevent tip-over instability. This adaptability is controlled by an optimization algorithm that updates the position of the mobile base with respect to the object, and accordingly, calculates a global arm configuration that minimizes the eccentricity of the external loading and maximizes the payload capacity of the arm.**

Keywords- Mobile Robot, adaptive manipulation, field testing, global optimization

I. INTRODUCTION

THE incorporation of robots in a human-inhabited environment is a trend that continues to thrive given the significant role that robots play in augmenting human faculty. The ability of the robot to accomplish tasks without fear or objection is especially desirable for the execution of missions in dangerous conditions, such as in hostile military environments. In military applications specifically, the use of field robots is becoming increasingly important because of the potential they hold in reducing the soldiers' exposure to dangerous scenarios, such as combat missions and land mines.

However, the substitution of soldiers by robot fighters also imposes significant engineering challenges. For instance, the unstructured nature of a realistic urban setting requires the robot to avoid [1]–[3] or adapt to obstacles that are present in this environment. Such obstacles include stairs, sidewalk ramps or any other types of urban architecture. Furthermore, the interaction of the robot with the surroundings can only be accomplished if the robot is equipped with a manipulator arm. This imposes additional challenges that relate to the motion control of the arm, the autonomy level of the end-effector and the dynamic balance of the robot during real-time sensor-based manipulation.

To address aspects of these issues, a hybrid mobile robot was proposed [4]–[7] that is capable of overcoming architectural obstacles by deploying its arm as a leverage. A second generation of this robot, called the HMMR (Hybrid Mechanism Mobile Robot) (Fig. 1), was developed to enhance the manipulation capabilities of the arm and strengthen the on-board sensorial and computational capacity necessary for the execution of autonomous maneuvers such as adaptive manipulation and dynamic stability.

In the context of stability, the balance of a mobile robot during manipulation is dictated by the tilting moment the arm and the eccentric load created around the pivot axis of the mobile platform. In the event where this moment exceeds the stabilizing moment generated by the platform's weight, the robot will have the tendency to lose balance and tip over. Thus, for real-time mobile robotic applications, it becomes critical to equip the robot with the appropriate sensing means and algorithm that enable the mobile base to detect the potential onset of dynamic destabilization, and adapt to it in order to lessen the risk of tip-over instability.

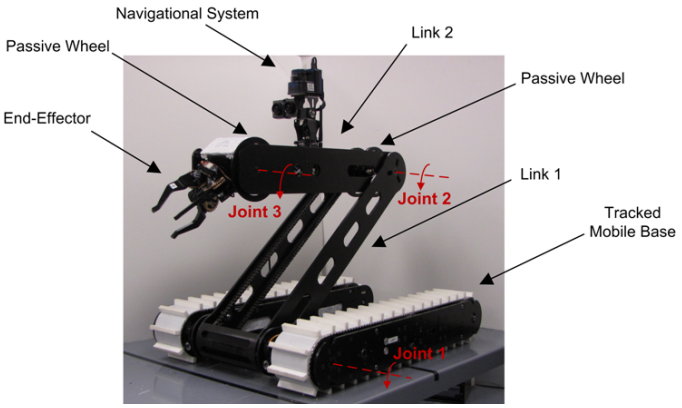

Figure 1. A prototype of the HMMR showing the navigational system, the mobile base, the arm and the end-effector

In this direction, this paper addresses the problem of obstacle avoidance and adaptive manipulation from an experimental and an analytical perspective. In the first section

This work was supported in part by the Defense Advanced Research Projects Agency (DARPA) under grant # HR0011-09-1-0049 and the Department of Mechanical and Aerospace Engineering at the George Washington University, Washington DC.

978-1-4577-0820-6/11/$26.00 ©2011 IEEE

of the paper, we discuss critical details of the HMMR's hardware layout and present experimental results that validate the ability of the robot to use its arm as a leverage to negotiate tall obstacles. In the second section, we focus on the adaptive manipulation capabilities of the HMMR, and introduce an algorithm that enables the robot to adapt its position and arm posture to the external load in order to maintain the dynamic balance of the mobile base. The effectiveness of the proposed algorithm is further demonstrated through simulation results derived from a case-study manipulation scenario.

II. HARDWARE LAYOUT OF THE HMMR

The HMMR's tracked platform possesses the overall dimensions of 530(W)×630(L)×140(H) mm and a measured static weight of 51Kg. The driving mechanism consists of two identical tracked units (Fig. 1), left and right, each driven independently by one motor M_1 through a planetary gearbox (ratio 32:1), a bevel gear (ratio 3:1) and a pulley assembly (Fig. 2-A). Motor M_1 is a brushless DC motor operating at 48 Volts and providing a peak power of 210 Watts with a maximum motor shaft speed of 9200 RPM and a peak torque at the pulleys of 27 N·m. In addition to the two tracked driving units, the HMMR carries a central dual-link manipulator arm cascaded between the tracks in a way to maintain the morphological symmetry of the platform. This symmetry allows the robot to achieve mobility under flip over conditions and is ideal for operation on rugged terrain where the risk of tipping is always present.

The central arm consists of two actuated joints and a three-finger end-effector. The two joints of the serial arm are revolute and are actuated by two brushless electrical motors M_2 located under the timing belts on both sides of the arm (Fig. 2-B). Motors M_2 provide a peak torque of 150 N·m at 8 RPM after three stages of amplification consisting of a harmonic drive (ratio 120:1), a bevel gear (ratio 3:1) and a sprocket-chain assembly (ratio 2.9:1). The left motor drives the lower joint (joint 1), while the right motor drives the upper joint (joint 2) through a chain transmission that runs along the length of link 2. The shafts of joint 2 and 3 further carry a set of passive wheels (Fig. 1) that rotate freely around their respective axis. Revolute joints 1 and 2 of the arm have endless rotation, where link 3 can complete a full rotation inside link 2, and link 2 can complete a full rotation inside the tracked units allowing the arm to deploy from either side of the robot for symmetry purposes.

The end-effector on the other hand contains three fingers and three joints (Fig. 3), two of which achieve the flexion/extension (joint 3) and pronation/supination (joint 5) maneuvers while the third achieves the opening/closing maneuvers of the three fingers (joint 4). The end-effector of the HMMR is designed as a self-contained entity of the robot as shown in Figure 3, where all motors, controllers, batteries and sensors are carried inside its structure. The three joints are actuated via brushless electrical motors operating at 20 Volt each, and enabling a peak torque of 20 N·m and a peak rotational speed of 75 deg/sec at the joint axes after two torque amplification stages consisting of planetary gears and worm gear assemblies that further ensure the non-back-drivability of the joints. Additional details of the structural features of the HMMR, as well as comparative analyses between the HMMR's characteristics and other state-of-the-art mobile platforms can be found in [5] – [8].

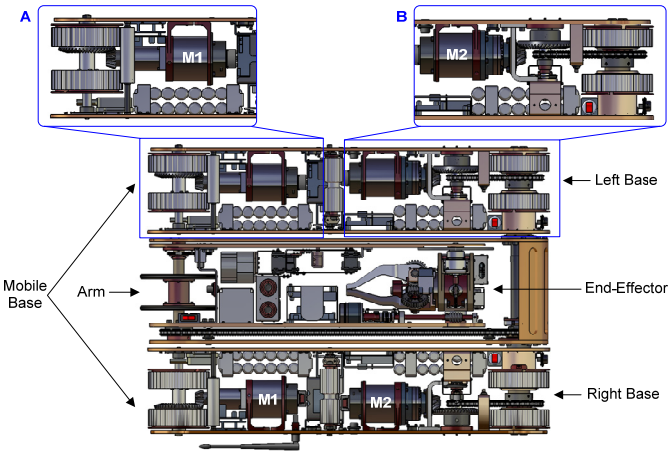

Figure 2. A top view of the hardware layout of the HMMR with the tracks hidden

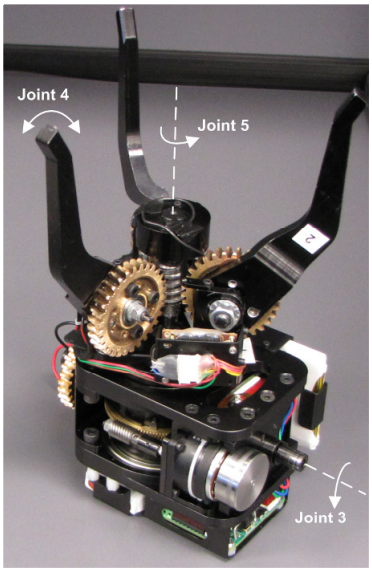

Figure 3. The self-contained end-effector of the HMMR showing all three joints

III. FIELD TESTING: CLIMBING AND DESCENDING OBSTACLES

Two sample maneuvers executed by the HMMR are demonstrated in Figures 4 and 5. These maneuvers consist of climbing and descending an obstacle whose height is much taller than the folded height of the robot. To achieve this, the robot uses its arm to leverage the symmetric tracked platform over the obstacle during climbing, or to support the platform during obstacle descending.

A. *Obstacle Climbing*

The process of obstacle climbing begins by positioning the robot in front of the obstacle (Fig. 4-a). The location of the robot is adjusted depending upon the height of the obstacle. A tall obstacle requires the robot to be positioned at the close

proximity of the obstacle's edge plane, while a shorter obstacle enables more positioning freedom. In any case, the second step in the process involves the rotation of the tracked units around joint 1 while maintaining contact between link 2 and the ground. This prevents the rotation of link 2 and causes the tracked units to rotate instead (Fig. 4-b), and this rotation is maintained until contact with the obstacle's edge is achieved (Fig. 4-c). The obstacle is assumed to be unyielding and stable enough to not slide away under the induced load of the robot (which is the case of many architectural obstacles found in the real-world). In this position, the stability of the platform is achieved by maintaining contact with the ground through link 2, and with the obstacle through the tracked units (Fig. 4-c).

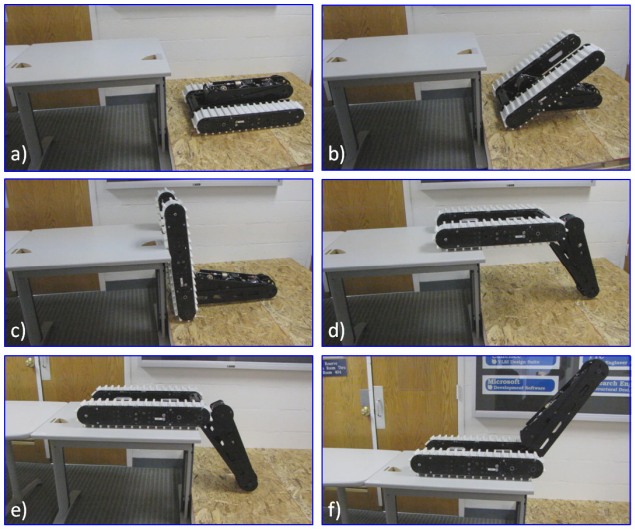

Figure 4. A sequence of maneuvers executed by the HMMR to climb an obstacle in a concession of processes using the manipulator arm as leverage

In this posture, the continued actuation of joint 1 causes the tracked base to rotate even further until the tracks lie flat on the top surface of the obstacle (Fig. 4-d). This provides enough traction for the tracks to move forward over the obstacle's top surface while link 2 maintains rigid contact and stable balance with the ground through the passive wheels (Fig. 4-e). The relevance of the passive wheels located on the shaft of joint 2 can be noted in this process, where they roll freely on the ground driven indirectly by the forward motion of the tracks to reduce the friction between link 2 and the ground. Once the tracked platform is stably positioned on top of the obstacle, the process of rotating link 2 back inside the tracks can be initiated (Fig. 4-f). We note that link 3 does not contribute to the sequences required to accomplish this maneuver as joint 2 remains idle during the climbing process.

B. Obstacle Descending

For any robot with obstacle climbing capabilities, the process of overcoming an obstacle should be reversible; meaning that the robot should be able to descend the obstacle in a rather similar but reversed sequence of maneuvers as in the ascending process. For the HMMR, this is accomplished by deploying the arm to support the tracked platform during the descending process, as highlighted in the case-study scenario of the robot descending a table shown in Fig. 5.

This process starts by positioning the robot at the obstacle's edge (Fig. 5-a). Link 2 of the manipulator arm is then rotated around joint 1 until contact with the ground is achieved through the passive wheels located on the shaft of joint 2 (Fig. 5-b). The tracked units are actuated forward thereafter until they clear the edge of the obstacle, using the arm and the passive wheels on the ground for balance and support (Fig. 5-c).

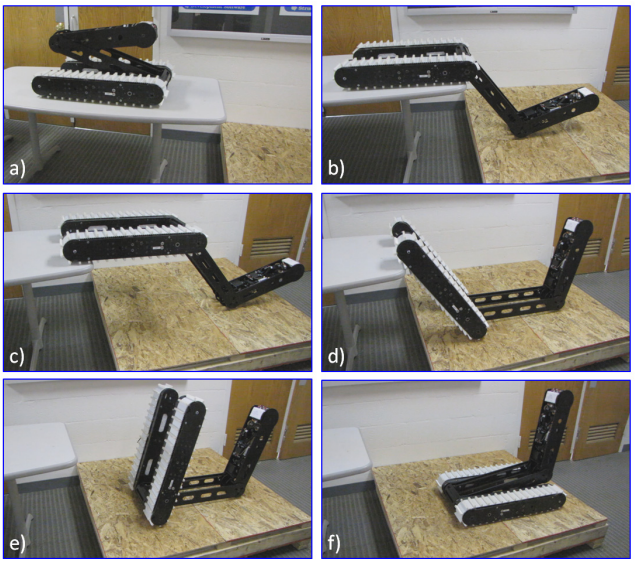

Figure 5. A sequence of maneuvers executed by the HMMR to descend an obstacle in a concession of processes using the manipulator arm as support

In this posture, the actuation of joint 1 allows the tracked units to rotate downwards about the joint, while link 2 continues to move forward using the passive wheels as a rolling support (Fig. 5-d). During this descending maneuver, balance is ensured through the wheels and the tracks maintaining contact with the obstacle's edge. The forward motion of the passive wheels, and subsequently the arm, enables the tracked units to collapse downwards until contact between the tracks and the ground is established (Fig. 5-d). In this position, link 2 of the arm is completely parallel to the ground. This means that the actuation of joint 1 starting from this posture will enable the tracked units to rotate away from the obstacle's edge and towards the arm which maintains balance during this maneuver (Fig. 5-e). The actuation of joint 2 is maintained until the tracks are leveled with the ground (Fig. 5-f).

IV. MANIPULATION: KINEMATICS AND REDUNANCY RESOLUTION

To analyze the kinematics of the HMMR's arm, we first present a schematic of its geometry in Figure 6, which shows the dimensions and the degrees of freedom of the arm. The geometric and structural characteristics of the robot are as summarized in Table 1, where we refer to the end-effector as Link 3, and where Θ_i denotes the angle of joint i measured with respect to the x-axis. l_i denotes the length of link i and l_{ci} denotes the location of the center of mass of link i measured with respect to joint i.

TABLE I. MASS AND GEOMETRIC CHARACTERISTICS OF THE HMMR'S ARM AND BASE

Link	Mass M (kg)	Link Length l (mm)	Center of Mass distance l_c (mm)
Base (0)	38.69	630	274
1	5.05	630	326
2	5.82	513	273
3	2.11	194.6	40.2

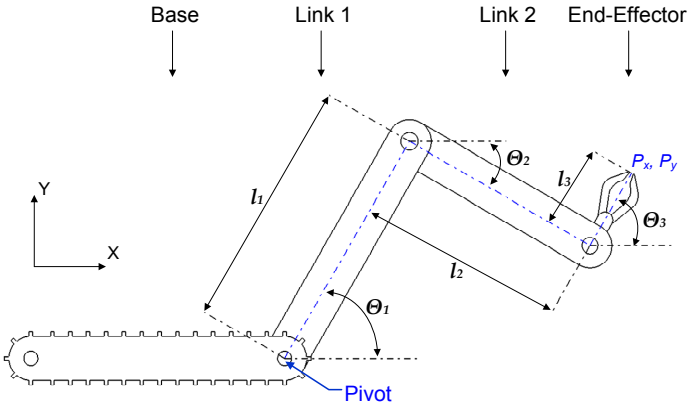

Figure 6. A schematic of the HMMR showing geometrical characteristics and degrees of freedom

With these structural characteristics, the tilting moment that the arm's static weight generates around the base pivot is written in a conservative form in terms of the arm's geometry and degrees of freedom as follows

$$\eta(\Theta) = \sum_{i=1}^{n} M_i l_{ci} \cos(\Theta_i) + \sum_{i=1}^{n-1} \left(\sum_{k=i+1}^{n} M_k \right) l_i \cos(\Theta_i) \quad (1)$$

where $\eta(\Theta)$ denotes the tilting moment and n denotes the number of joints. For n=3, equation (1) can be further simplified into an expression with a single factored-out summation term as

$$\eta(\Theta) = \sum_{i=1}^{2} \left\{ M_i l_{ci} + \left(\sum_{k=i+1}^{3} M_k \right) l_i \right\} \cos(\Theta_i) + M_3 l_{c3} \cos(\Theta_3) \quad (2)$$

The forward kinematics of the end-effector position in the X-Y plane denoted by coordinates P_x and P_y can also be written in a conservative form in terms of the joint angles as follows

$$\begin{aligned} P_x &= \sum_{i=1}^{3} l_i \cos(\Theta_i) \\ P_y &= \sum_{i=1}^{3} l_i \sin(\Theta_i) \end{aligned} \quad (3)$$

From equation (3), it is obvious that the end-effector position in the planar workspace is a function of three joint variables. This generates a kinematic redundancy of order 1, and prevents a closed form solution of the inverse kinematic problem for autonomous end-effector placement maneuvers.

To resolve this redundancy, we convert equations (2) and (3) into a minimization problem where the objective is to minimize the effect of the tilting moment subject to the forward kinematics, which are now regarded as equality constraints. This problem can be formulated mathematically as follows

$$\begin{aligned} &\underset{\Theta}{Min} \quad \eta(\Theta) \\ &subject\ to \quad h_1(\Theta) = P_x - \sum_{i=1}^{3} l_i \cos(\Theta_i) = 0 \\ &\qquad\qquad\ \ h_2(\Theta) = P_y - \sum_{i=1}^{3} l_i \sin(\Theta_i) = 0 \end{aligned} \quad (4)$$

Resolving kinematic redundancy can traditionally be done using methods such as the pseudo-inverse [10], extended Jacobian [11], [12] and matrix decomposition [13]. Although the efficacy of such methods is well proven, their solution is often characterized by the locality of the optimum as opposed to globality. However, when the objective is to maintain the dynamic balance of the mobile base during manipulation, finding the global optimum of the cost function becomes critical since the difference between the locality and globality of the solution could mean the difference between whether the robot maintains stability during manipulation maneuvers, or whether the arm's posture and the longitudinal eccentricity of the external load cause the robot to lose balance and tip-over.

In this line of thought, we opt at resolving problem (4) as an explicit global minimization problem where we first append the equality constraints $h(\Theta)$ to the cost function $\eta(\Theta)$ using Lagrange multipliers λ

$$L(\Theta) = \eta(\Theta) - \lambda^T h(\Theta) \quad (5)$$

and then solve the simultaneous system of non-linear equations resulting from the first derivative, $\nabla L = 0$

$$\begin{bmatrix} -(M_1 l_{c1} + M_2 l_1 + M_3 l_1)\sin(\Theta_1) + \lambda_1 l_1 \sin(\Theta_1) - \lambda_2 l_1 \cos(\Theta_1) \\ -(M_2 l_{c2} + M_3 l_2)\sin(\Theta_2) + \lambda_1 l_2 \sin(\Theta_2) - \lambda_2 l_2 \cos(\Theta_2) \\ -M_3 l_{c3} \sin(\Theta_3) + \lambda_1 l_3 \sin(\Theta_3) - \lambda_2 l_3 \cos(\Theta_3) \\ X - l_1 \cos(\Theta_1) - l_2 \cos(\Theta_2) - l_3 \cos(\Theta_3) \\ Y - l_1 \sin(\Theta_1) - l_2 \sin(\Theta_2) - l_3 \sin(\Theta_3) \end{bmatrix} = 0 \quad (6)$$

using a numerical method. This method is developed using a Newton step where the first-order Taylor series expansion of $L(\Theta)$ in (5) given by

$$\nabla L(q^{k+1}) = \nabla L(q^k) + \frac{\partial}{\partial q} \nabla L \Big|_{q^k} \delta q^k \quad (7)$$

generates a gradient descent indexed by k with $\nabla L(q^{k+1}) = 0$, of the size

$$q^{k+1} = q^k - H^{-1} \Big|_{q^k} \nabla L \Big|_{q^k} \quad (8)$$

with

$$q = \begin{bmatrix} \Theta \\ \lambda \end{bmatrix} \in \mathbb{R}^{5\times 1} \quad (9)$$

and $H = \frac{\partial^2 L(\Theta)}{\partial^2 q}$ representing the Hessian matrix of (5).

Finding the global solution of (6) using the iterative step of (8) is achieved by searching the configuration space incrementally (10° increment) for all local minima and retrieving the absolute minimum of them. While this could be a relatively slow process for on-line sensor-based applications, it is possible to accelerate the convergence rate of this solution by exploring the unique characteristics of the system of equations presented in (6). By limiting the search space to the practical configuration space of the arm defined by

$$\begin{aligned} 0 < \Theta_1 < 151° \\ -90 < \Theta_3 < 90° \end{aligned} \tag{10}$$

where Θ_2 is indirectly bounded by (10); it is possible to start the iterative solution of (6) near an optimum by deriving analytical expressions for the initial guess of λ_1 and λ_2 from the first and third equations in matrix $\nabla L = 0$ in (6) using an initial guess of Θ_1^{init} and Θ_3^{init} in the search space of (10). These expressions are as follows

$$\begin{aligned} \lambda_1^{init} &= \frac{ce - bf}{ae - bd} \\ \lambda_2^{init} &= \frac{cd - af}{ae - bd} \end{aligned} \tag{11}$$

with

$\boldsymbol{a} = l_1 sin(\Theta_1^{init})$; $\boldsymbol{b} = l_1 cos(\Theta_1^{init})$;

$\boldsymbol{c} = (M_1 lc_1 + M_2 l_1 + M_3 l_1)\, sin(\Theta_1^{init})$;

$\boldsymbol{d} = l_3 sin(\Theta_3^{init})$; $\boldsymbol{e} = l_3 cos(\Theta_3^{init})$; $\boldsymbol{f} = M_3 l_{c3}\, sin(\Theta_3^{init})$

Furthermore, using (11), it is also possible to derive an additional analytical expression for the initial guess of Θ_2 from the second equation in matrix $\nabla L = 0$ in (6). This equation can be written as

$$\Theta_2^{init} = \tan^{-1}\left\{ \frac{\lambda_2^{init} l_2}{\lambda_1^{init} l_2 - M_2 l_{c2} - M_3 l_2} \right\} \tag{12}$$

The advantage of initializing the search algorithm with (11) and (12) is reflected in Figure 7. In this figure, we compare the number of iterations prior to local convergence for 100 attempts initialized using random guesses of λ and Θ_2, to the number of iterations prior to local convergence with an initial estimate of λ and Θ_2 made according to (11) and (12), respectively. In all 100 cases, the initial start for Θ_1 and Θ_3 was maintained. As can be seen in this figure, the choice of λ and Θ_2 according to (11) and (12) generates a faster local convergence in 98% of the cases. This accelerates the search across the configuration space for the global minimization of (5), and enables us to employ the gradient-based algorithm to explore the adaptive manipulation capabilities of the HMMR in real-time sensor-based applications.

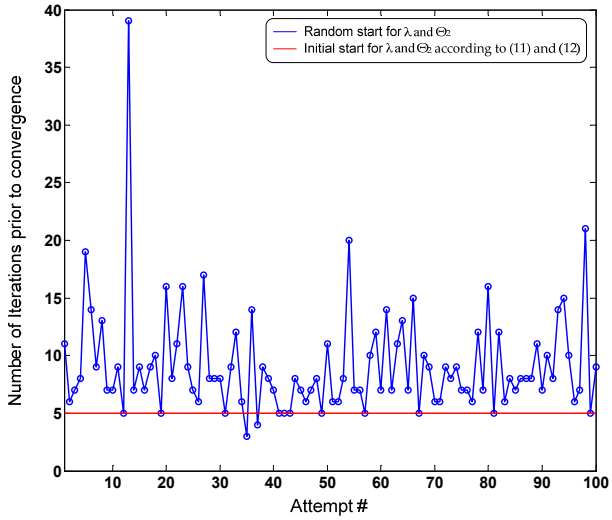

Figure 7. Number of iterations required prior to convergence for a random choice of λ and Θ_2, vs. a choice of λ and Θ_2 made according to (11) and (12), respectively

V. ADAPTIVE MANIPULATION

In the previous discussion, the objective of the minimization algorithm was to resolve the kinematic redundancy of the arm for a desired end-effector task, and generate a posture that maximizes the payload capacity of the manipulator by minimizing the tilting moment the arm's weight generates around the base pivot. In practical applications, the minimization problem must also account for the weight of the object at the end-effector and its contribution to the tilting moment and the stability of the robot.

Measuring the weight of the object carried by the arm can be done using a force sensor incorporated at the end-effector's fingers. In a gravity-governed environment, the external load induced by the weight of the object increases progressively from zero when the object is completely on the ground until load saturation when the object is fully carried by the arm. This behavior is shown in Figure 8 where a progression of manipulation maneuvers is matched with the corresponding progressive object load induced onto the arm at the end-effector. By converting this continuous progression into a discrete sequence of sensor readings at instances m, it is possible to trigger the minimization algorithm to reposition the robot with respect to the object in order to minimize the eccentricity of the external load, and accordingly, recalculate a new joint posture that maximizes the arm's payload capacity.

Triggering the algorithm to reposition the robot with respect to the object is achieved anytime the condition

$$M_0 lc_0 - \delta\eta > \eta(\Theta) + FP_x \tag{13}$$

is violated. In (13), M_0 denotes the mass of the base, l_{c0} denotes the location of the base center of mass with respect to the pivot and $F \triangleq F(m)$ represents the measured instance of the external load. $\delta\eta$ is added as a safety margin to the stabilizing moment ($\delta\eta$ =2 N·m in this application).

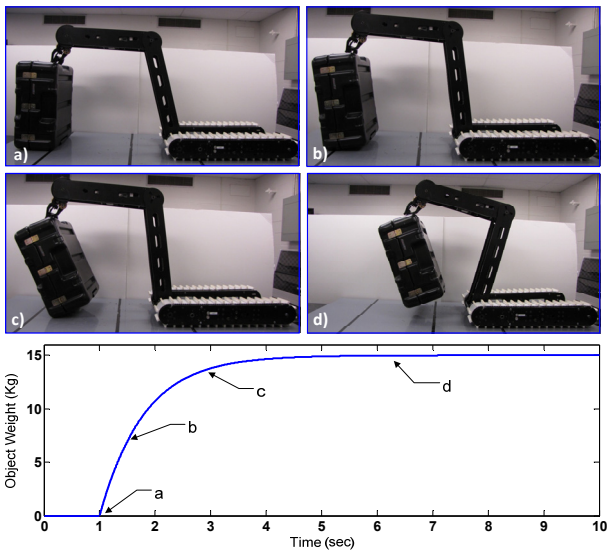

Figure 8. A progression of manipulation sequences with corresponding increase of the external load on the arm

Every time equation (13) is violated, a new value *X(m)* is calculated based on

$$X(m) = \frac{(M_0 l_{c0} - \delta\eta) + \eta(\Theta)}{F(m)} \qquad (14)$$

and the algorithm automatically moves the base closer towards the object by *X(m-1) – X(m)* and recalculates a new posture of the arm based on the minimization problem of (4). This procedure is simulated in Figure 9 for a 15 Kg payload located at P_x= 0.9 m and P_y= 0.4 m.

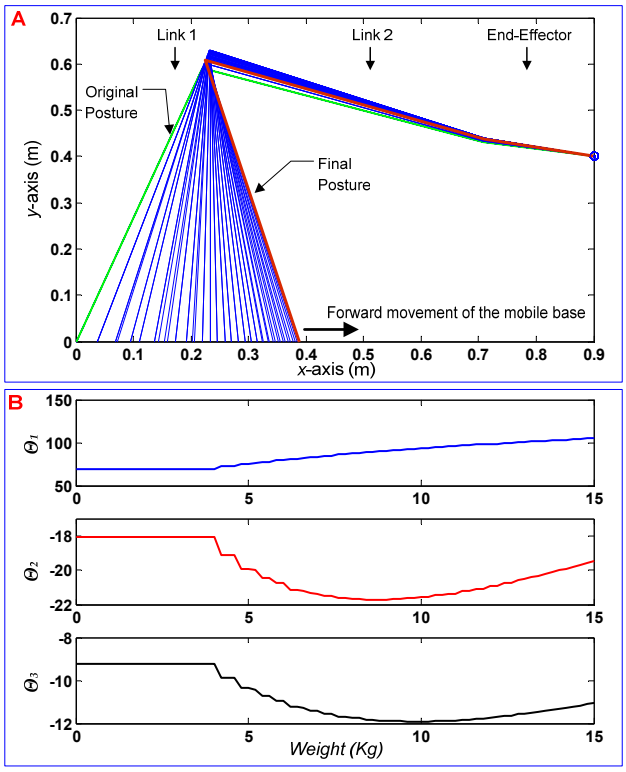

Figure 9. Simulation of the forward movement of the arm (A) and the corresponding joint history after reconfiguration (B).

In Figure 9-A, the base is originally located between coordinates 0.63m and 0m, and condition (13) is first violated at *F*=4.5Kg. Thereafter, Figure 9-A shows the forward movement of the arm under incremental instances of external loading, while Figure 9-B shows the joint history of the arm's reconfiguration as a result of the forward movement.

VI. CONCLUSION

This paper presented the field testing results and adaptive manipulation of a hybrid mechanism mobile robot (HMMR). The algorithm discussed in the paper maximizes the payload capacity of the arm and enables the robot to reposition the mobile base to avoid tipping over under excessive external loading. In the future work, we will validate the effectiveness of the algorithm in a closed loop control scheme involving the force sensor at the end-effector and the mobile base actuators.

REFERENCES

[1] N. Uchiyama, T. Hashimoto, S. Sano, and S. Takagi, "Model-Reference Control Approach to Obstacle Avoidance for a Human-Operated Mobile Robot," *IEEE Transactions on Industrial Electronics*, vol. 56, no. 10, pp. 3892 – 3896, October 2009.

[2] J.H. Lilly, "Evolution of a Negative-Rule Fuzzy Obstacle Avoidance Controller for an Autonomous Vehicle," *IEEE Transactions on Fuzzy Systems*, vol. 15, no. 4, pp. 718 – 728, August 2007.

[3] M.J. Er, and C. Deng, "Obstacle Avoidance of a Mobile Robot Using Hybrid Learing Approach," *IEEE Transactions on Industrial Electronics*, vol. 52, no. 3, pp. 898 – 905, June 2005.

[4] P. Ben-Tzvi, A.A. Goldenberg, and J.W. Zu, "Design and Analysis of a Hybrid Mobile Robot Mechanism with Compounded Locomotion and Manipulation Capability," *Transactions of the ASME, Journal of Mechanical Design*, vol. 130, pp. 1 – 13, July 2008.

[5] P. Ben-Tzvi, A.A. Goldenberg, and J.W. Zu, "Articulated Hybrid Mobile Robot Mechanism with Compounded Mobility and Manipulation and On-Board Wireless Sensor/Actuator Control Interfaces," *J. Mechatronics*, vol. 20, no. 6, pp. 627 – 639, September 2010.

[6] P. Ben-Tzvi, "Experimental Validation and Field Performance Metrics of a Hybrid Mobile Robot Mechanism," *Journal of Field Robotics*, vol. 27, no. 3, pp. 250 – 267, May 2010.

[7] P. Ben-Tzvi, A.A. Goldenberg, and J.W. Zu, "Design, Simulations and Optimization of a Tracked Mobile Robot Manipulator with Hybrid Locomotion and Manipulation Capabilities," *in Proc. of the IEEE International Conference on Robotics and Automation*, ICRA '08, Pasadena, California, 2008, pp. 2307 – 2312.

[8] P. Moubarak, P. Ben-Tzvi, and Z. Ma, "A Mobile Robotic Platform for Autonomous Navigation and Dexterous Manipulation in Unstructured environments," *Proceedings of the ASME International Mechanical Engineering Congress and Exposition (IMECE 2010)*, Vancouver Canada, November 2010.

[9] P. Moubarak, P. Ben-Tzvi, and Z. Ma, "A Generic Configuration of a Compact Dexterous and Self-Contained End-Effector for Mobile Robotic Platforms," *Proceedings of the IEEE International Workshop on Robotic and Sensors Environments (ROSE 2010)*, Phoenix, AZ, 2010, pp. 1 – 6.

[10] J. Park, Y. Choi, W.K. Chung, and Y. Youm, "Multiple tasks kinematics using weighted pseudo-inverse for kinematically redundant manipulators," *in Proc. of the IEEE International Conference on Robotics and Automation*, ICRA '01, Korea, 2001, pp. 4041 – 4047.

[11] K. Tchon, "Optimal Extended Jacobian Inverse Kinematics Algorithms for Robotic Manipulators," *IEEE Transactions on Robotics*, vol. 24, no. 6, pp. 1440 – 1445, December 2008.

[12] K. Tchoń, "Repeatable Extended Jacobian Inverse Kinematics Algorithm for Mobile Manipulators," *Systems & Control Letters*, vol. 55, no. 2, pp. 87 – 93, February 2006.

[13] M. Tarokh, and M. Kim," Inverse Kinematics of 7-DOF Robots and Limbs by Decomposition and Approximation," *IEEE Transactions on Robotics*, vol. 23, no. 3, pp. 595 – 600, June 2007.